

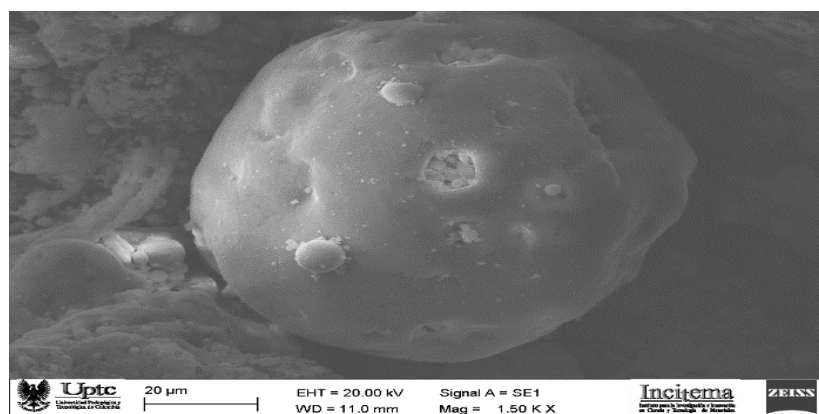
Full Paper | <http://dx.doi.org/10.17807/orbital.v25i2.18260>

# Structural, Morphological and Physical Characterization of Carbon Fly Ash

Ricardo Parra-Huertas\* <sup>a</sup>, Carlos Calderón-Carvajal <sup>a</sup>, and Jairo Gómez-Cuaspad <sup>a</sup>

Carbon fly ash (CFA) is the principal industrial waste byproduct from the burning fossil fuel (coal combustion) for the thermal generation of electricity. CFA is a gray or black powdery solid that is constituted mostly metal oxides (Al, Si Fe and Ca), unburned carbon (UC) and other inorganic substance. The management of fly ash has thus been a matter of concern given the requirement of the large area of land for its disposal and potential of causing pollution of air, water, land and effects on human health. Physical and chemical characteristics of fly ash is important, as these characteristics influence its subsequent use and disposal. X-ray diffraction, and fluorescence, scanning microscopy with an energy dispersive spectroscopy, FTIR, BET was the common techniques employed to characterize FA. Characterization by XRD analysis identified the presence of quartz, mullite and sillimanite phases; while the FTIR results allowed the identification of vibrational bands, characteristic of Si-O-Si and Si-O bonds. The EDS analysis coupled to SEM allowed verifying that the composition of the samples is consistent with the results sought and that the morphological characteristics validate the proposed methodology. Surface area analyses (BET) showed that the fly ash possess an active area of  $6.02 \text{ m}^2 \cdot \text{g}^{-1}$ .

## Graphical abstract



## Keywords

Aluminosilicates  
Coal  
Characterization  
Fly ash  
Waste

## Article history

Received 22 Mar 2023  
Revised 30 May 2023  
Accepted 30 May 2023  
Available online 13 Jul 2023

Handling Editor: Cauê Martins

## 1. Introduction

The main goal of sustainable development is to achieve better future for future generations by creating sustainable economic, industrial, social, growth and seeking ways to protect the environment. Unfortunately, industrialization, urbanization and intensification of agriculture reveals steadily increasing levels of pollution in our environment [1]. Is so that

in the past few decades, prosperity in economy and human life has demanded huge energy consumption [2]. Some energy sources are derived from fossil fuel and renewable sources including solar, wind, hydropower and biomass [2, 3], biofuels, waste, natural gas combustion, oil combustion and coal combustion [3].

<sup>a</sup> Escuela de Ciencias Químicas, Química. Grupo de Integridad y Evaluación de Materiales (GIEM). Instituto para la Investigación e Innovación en Ciencia y Tecnología de Materiales (INCITEMA), Universidad Pedagógica y Tecnológica de Colombia, Av. Central del Norte 39-115, Tunja, Colombia. \* Corresponding author. E-mail: [ricardo.parra@uptc.edu.co](mailto:ricardo.parra@uptc.edu.co)

Regarding the latter more than 40 % of the global electric power generation relies on the burning of coal [4, 5], in addition to being the second most used fossil fuel and more important, compared to other kinds of energy [3, 6, 7]. The reserves are approximately one trillion tons [7], making coal combustion an important process for generation electricity in many countries, however when burned in thermal power plants, its generate residues in form of tiny particles which are carried by combustion gases. Such residues are called fly ashes and are collected by filter systems [7] and large amounts are generated during coal combustion, it is estimated that in coal-fired power plants, every 2 ton of coal produces 1 ton of CFA [3].

Fly ash is alkaline, abrasive [8], mainly composed of fine-grained [9, 1] and spheres or hollow spheres with a diameter of 1-100  $\mu\text{m}$  [10, 1] composed of spherical aluminosilicate glass particles, formed as a result of burning coal to 1200-1700  $^{\circ}\text{C}$  in thermal power plants [1, 11] and collected by electrostatic precipitators from the flue gases in thermal power plants [12]. The color depends on the mineral composition of coal source, it may have a dark, gray or black color [13].

The chemical composition of CFA resulting from hard coal combustion comprises mostly silicon, aluminum, iron in the form of oxides and quartz, mullite, hematite and magnetite are the most frequently occurring crystalline phase [8, 9, 14-18].

A large amount of fly ash is idle or abandoned, resulting in severe environmental and ecological problems [4,19] and has become one of the largest sources of industrial solid waste [20]. The fly ash causes a series of problems such as water pollution, air pollution, land pollution and health effect [3, 4, 16, 20, 21, 22], with ecological risk due to the infiltration and accumulation of toxic elements in the soil such as Se, As, B, V, Al, Pb, Hg, Cr [1, 8, 12, 23]. In addition to above causes serious health hazards by inhalation of fine particulate matter, influencing the DNA repair mechanism due to PAHs (polycyclic aromatic hydrocarbons) derived from unburnt organic matter. Small particles from coal-fired power plants and storage sites can reach the brain indirectly through the lungs and bloodstream or directly through the olfactory bulb causing neurobehavioral symptoms [12], in addition to being considered a human carcinogen [17].

The most important measure to reduce CFA is to add it into construction materials due to its pozzolanic properties, adsorbents, catalyst, soil remediator, mitigate heavy metals emissions [3]; construction materials, e.g. additives for cement [4, 10, 23, 26-31] synthesis of zeolites [4, 10, 23, 30, 31], ceramic production; agriculture [16, 30, 32-34], geopolymers [4, 10, 16, 30] and carbon nanotubes [35].

### Classification of coal fly ash

ASTM (American Society for Testing and Materials) has set a standard for CFA based on coal properties: CFA of class F, mainly obtained from anthracite or bituminous coal combustion, contains CaO below 10 % and possess pozzolanic properties only [31] and class C obtained from lignite or sub-bituminous coal combustion [3, 16, 31], contains CaO higher than 10 % and possess cementitious and pozzolanic properties [31]. The table 1 shows that in the ASTM classification Class F CFA has a combined  $\text{SiO}_2$ ,  $\text{Al}_2\text{O}_3$ , and  $\text{Fe}_2\text{O}_3$  content more than 70 % [16, 24, 36]; while Class C contains more than 50 % of combined  $\text{SiO}_2$ ,  $\text{Al}_2\text{O}_3$ , and  $\text{Fe}_2\text{O}_3$  oxides [34].

The United Nations (UN) classifies CFA into four groups according to  $\text{SiO}_2/\text{Al}_2\text{O}_3$  ratio and CaO content, where Group-I

CFA have  $\text{SiO}_2/\text{Al}_2\text{O}_3 \geq 2$  and CaO amount up to 15 %. Group II includes CFA with  $\text{SiO}_2/\text{Al}_2\text{O}_3$  ratio of up to 2 and CaO amount  $\geq 15$  % with  $\text{SO}_3$  content  $\leq 3$  %. The Group III CFA, in contrast, has the amount of CaO and  $\text{SO}_3$  more than 15 % and 3 % respectively, while the Group IV includes CFA with CaO amount more than 15 % with  $\text{SO}_3$  less than 3 % [34, 37].

**Table 1.** Classification systems of the US and European standards bodies for the fly ash [34, 37].

Class	$\text{SiO}_2 + \text{Al}_2\text{O}_3 + \text{Fe}_2\text{O}_3$ (%)	$\text{SO}_3$ (%)	Moisture (%)
C	$\geq 50$	$\leq 5$	$\leq 3$
F	$\geq 70$	-	-

This study aimed to characterize fly ash, an industrial waste with significant potential for various industrial applications. Due to its chemical composition and unique characteristics, this type of ash holds great promise in material substitution, nanomaterial synthesis, environmental remediation, and numerous other fields.

## 2. Results and Discussion

### X-ray diffraction (XRD) analysis

X-ray diffraction is a powerful technique that detects the crystalline phases present in sufficient quantity in a sample. Fig. 1 presents the results of this analysis when crystalline phases are represented by peaks, while amorphous phase is represented by the hump. The images presented show a large amount of amorphous content which is so to be expected with fly ash, above 80% [38]. Fig. 1 shows the XRD pattern of fly ash, which indicates that the mineral phase of fly ash mainly consists of sillimanite, quartz and mullite. The presence of quartz and mullite in fly ash are reported by [12, 14, 25, 39, 40] and the presence of sillimanite. The presence of mullite in the sample shows that the combustion temperature in the boiler exceeded 1100  $^{\circ}\text{C}$  [41] and the broad hump between 20  $^{\circ}$  and 30  $^{\circ}$  of the fly ash is mainly due to the presence of amorphous silica [12].

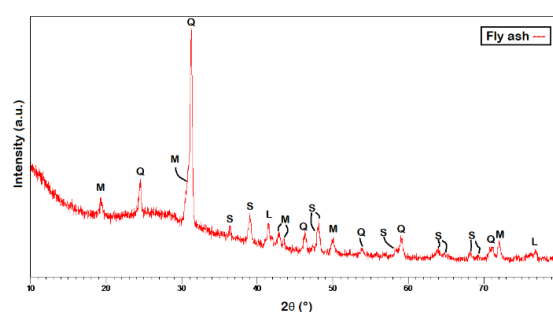


**Fig. 1.** X-ray diffraction pattern for the FA sample identifying the phases of M: mullite, Q: quartz, S: sillimanite and L: Lime.

Though the crystalline phase is not abundant, the present of quartz and mullite indicates the abundant of Si and Al in the coal fly ash [42].

The diffraction patterns shown in Fig 1 corresponding to fly ash structure reveal that this starting material has crystalline structures in its composition, which agree with the AMCS indexed patterns 0001059, 0011007, 0004110, 0008315 and 0000128, consistent with mullite (M), quartz (Q), sillimanite (S) and lime (L) phases. Indexing of the main signals in the pattern corresponding to fly ash revealed the

corresponding phases of mullite, quartz and sillimanite, found the most intense signals around  $30.05^\circ$ ,  $31.45^\circ$  and  $39.04^\circ$ ,  $2\theta$  respectively as indicated in preliminary cases [4, 21, 22]. The identification of such structures distributed along the diffraction pattern was based on the signals located above  $41.80^\circ$  and  $77.20^\circ$   $2\theta$  for the case of the lime phase.

#### Fourier Transform Infrared Spectroscopy (FTIR) analysis

As vibrational spectroscopy in the infrared region provides important information related to specific chemical bonds, it is helpful for evaluating. Fig 2 shows the infrared spectrum corresponding to CFA with its main vibrational bands, as detailed in Table 2. The results are in agreement with the work of [43, 44] regarding the vibrational bands responsible for the asymmetric T-O-T stretching signals (T = Si, Al), attributed to the main oxidic structures of this type of materials. These signals are characteristic of semi-crystalline amorphous of varied compositions and related to aluminosilicates as the main components of FA, which are generally evidenced by the oxygen bonds with different aluminum and silicon tetrahedral forming structures of different number of members [45].

The bands located above  $545$  and  $748\text{ cm}^{-1}$  are related to the symmetric and asymmetric modes of vibration of the tetrahedron formed by the Si-O-Si bonds [46], while the band located at  $1058\text{ cm}^{-1}$  is attributed to the antisymmetric stretching mode of vibration corresponding to the Si-O-Al bonds, as previously identified by [43, 45, 47].

Although it is true that all the analyzed signals agree with the chemical profile of these raw materials, it is clear that the inverse signal located above  $2854\text{ cm}^{-1}$  and  $2924\text{ cm}^{-1}$  was associated with the presence of unburned products that are not completely eliminated in the coal combustion processes and preliminary treatments. [48, 49] indicate that these signals correspond to CH stretching vibration.

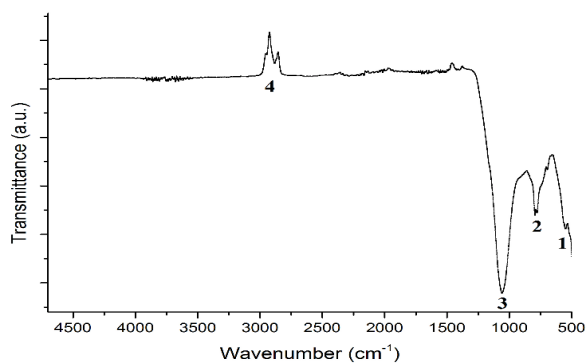


Fig. 2. Infrared spectrum of fly ash sample

Table 2. Transmittance signals for fly ash with its respective infrared active wavelength.

Band number	Wavelength (cm <sup>-1</sup> )	Type of bond
1	667	T-O-T (T = Si, Al)
2	748	Si-O-Si
3	1058	Si-O-Al
4	2854-2924	CH <sub>4</sub>

#### Scanning Electron Microscopy (SEM) analysis

SEM is an instrumental technique useful to characterize the spherical morphology of fly ash. As shown in the micrograph in Fig. 3, it reveals that the FA particles correspond to a spherical shape associated with amorphous aluminosilicate glassy material of

submicrometer size [12, 30, 40] and associated with high temperature during combustion of pulverized coal [50]. From the SEM picture, fly ash particles are mainly spherical with smooth surface and some irregular polymers [40], with several characteristics (microspheres, spheres and plerospheres) [5, 8] and cenospheres that contain smaller.

This spherical shape is the result of sudden cooling processes during the coal combustion process in the formation of FA [4, 51, 52].

According to [3, 40] the morphological characteristics of FA composed by amorphous silica, is related to a relatively smooth surface, which do not change after calcination, where there are no apparent micropores and holes on the surface, which is consistent with the results obtained from N<sub>2</sub> adsorption-desorption isotherms [53]. These morphologic structures correspond to mullite and quartz [54], in accordance with the XRD results, where it is clear that the amorphous coal fly ash is mainly composed by globular glass beads with different sizes, formed during the coal treatment at high temperatures in the gasification process as has been reported by [11].

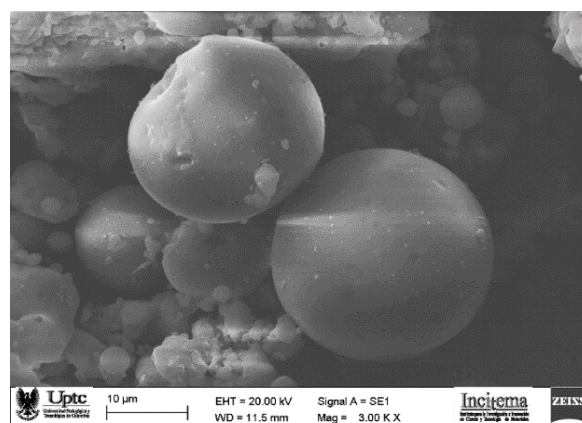


Fig. 3. Scanning electron microscopy image for fly ash.

#### Chemical composition analysis

The elemental composition of the FA was determined using the energy dispersive X-ray analysis (SEM-EDS), being consistent with the results found by structural characterization as shown in Fig 4. The elemental composition determined by EDS corresponds with the structural phases identified by diffraction analysis, where the FA is composed of C, Si, Al, O and Ca in 1.75, 32.20, 13.44, 50.54 and 2.07 % respectively. In this regard [32], reports percentage values of Si, Al and Ca of 11.18, 5.14 and 19.47 % respectively in the FA consistent with the composition of the raw material proposed in the current work [30], identifying in the fly ash Si, Al, Na, Fe and Ca [48], reports values of Si=28.21%, Al= 15.44, O=50.95 % and Ca=1.10 % and [12], reported presence of Si, Al, Ca, Fe.

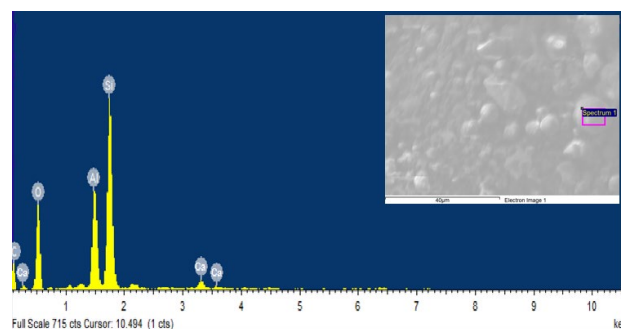


Fig. 4. EDS-type analysis of the fly ash.

### Textural properties analysis

The Figure 5- a shows the N<sub>2</sub> adsorption/desorption isotherms and pore size distribution curves of fly ash. The results confirm an uptake of N<sub>2</sub> increases steeply above the relative pressure of 0.95 for fly ash, showing a typical IV isotherm that is indicative of a mesoporous structure. The presence of the hysteresis loop at relative pressure ranging from 0.45 to 0.95 corresponding to type H3 of IUPAC classification, means that the particles are plate-like and have slit-like pores, this behavior is similar to reported by [35, 55] in the sample of fly ash. Is clear that the relative pressure of separation between adsorption curve and desorption curve exceeded the 0.4 value ( $P/P_0 > 0.4$ , where P is the adsorbent pressure and P<sub>0</sub> is the vapor pressure), indicating that this composite correspond to a mesoporous material. The absence of an inflection point demonstrates the absence of micropores in the sample analyzed [46], this is related with a low surface area of the fly ash  $6.02 \text{ m}^2 \cdot \text{g}^{-1}$ , these and others textural properties are listed in Table 3 in accordance with previous works in which the surface area for fly ash was  $1.4 \text{ m}^2 \cdot \text{g}^{-1}$  [56] and  $3.6 \text{ m}^2 \cdot \text{g}^{-1}$  [55].

The corresponding BJH adsorption method (Barrett, Joyner and Halenda, Fig. 5- b), show that the average pore size of the fly ash was 9.23 nm with pore sizes of 8.1 nm and average pore volumes of  $0.01 \text{ (cm}^3 \text{ g}^{-1}\text{)}$  for the fly ash in similar reaction conditions, validating the proposed synthesis method.

**Table 3.** Physical parameters of fly ash.

Sample	S <sub>BET</sub> (m <sup>2</sup> · g <sup>-1</sup> )	Micropore volume (t-plot) (cm <sup>3</sup> · g <sup>-1</sup> )	Pore Volume (cm <sup>3</sup> · g <sup>-1</sup> )	Pore size (nm)
Fly ash	6.02	0.00	0.01	9.23

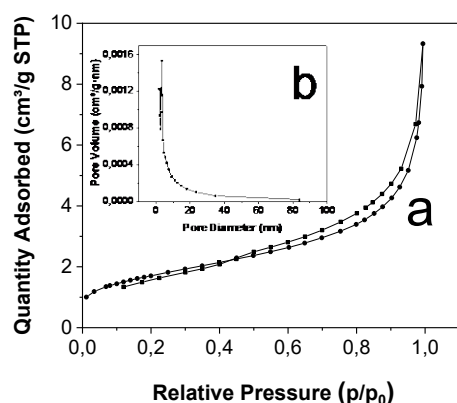


**Fig. 5.** Nitrogen adsorption-desorption isotherms for FA and pore volume distribution calculated by the Barret-Joyner-Halenda (BJH) method.

### 3. Material and Methods

The fly ash in the experiments was obtained from the Termopaipa station power plant (Boyacá, Colombia). The collected ash was dried at 90 °C for 24 h and subsequently taken to calcination at 700 °C in a TERRIGENO FPCA muffle furnace for 3 h at a heating rate of 1°C min<sup>-1</sup> to remove carbonaceous residues [4].

#### Characterization of the fly ash

The CFA was characterized by X-ray diffraction (XRD), infrared spectroscopy (FTIR), morphological (SEM), and compositional analysis by scanning electron microscopy coupled to X-ray dispersive analysis (EDS). The specific surface and pore volume of the fly ash were determined through a Brunauer-Emmett-Teller (BET) analyzer.

The structural characterization by X-ray diffraction technique was performed in an X'pert PANanalytical PRO-MPD equipment, equipped with an Ultrafast X'Celerator detector in Bragg-Brentano configuration using Cu K $\alpha$  radiation ( $\lambda = 1.54 \text{ \AA}$ ) between 10 and 90 ° with steps of 0.02 ° with a voltage of 40 Kv. The diffraction patterns obtained were indexed and analyzed in the X'Pert HighScore Plus software. Infrared spectroscopy (FTIR) analyses were performed between 4700-500 cm<sup>-1</sup> under Happ-Genzel apodization in a Shimadzu IRSpirit-T with a deuterium lamp and neon laser source in ATR configuration and a number of 20 scans. The morphological and compositional aspects were determined by scanning electron microscopy (SEM-EDS) in a RA-Zeiss-001 EVO-MA10 equipment furnished with Oxford X-ray dispersive spectrometry. In all cases, the distance between the electron gun and the sample was kept at 8.5 mm (WD). The applied energy was 20 kV and a secondary electron detector was used. The materials were prepared in an aluminum sample holder, using adhesive carbon disks and the samples coated with gold to reduce the static charge and improve the quality of the images. For the specific surface area and pore size distribution, nitrogen sorption/desorption measurements were carried out with a Micromeritics instrument ASAP 2020. Prior to the analysis, the samples were submitted to a cleaning step for 6 h in a vacuum a 150 °C. Mathematic models were employed Brunauer-Emmett-Teller (BET) and Barrett-Joyner-Halenda (BJH) to determine the surface area and pore date.

### 4. Conclusions

The results obtained from this chemical, structural, morphological, physical study confirm the fact that the coal fly ash located at the thermoelectric power station in Paipa-Colombia have high percentage oxides of Si, Al, Fe and Ca and therefore makes them good candidates for industrial application. With the problem of ash management and leachate contamination of groundwater, fly ash disposal on land or lagoons should be discouraged. This study has instead provided information to enable sustainable use of coal fly ash in various fields such as synthesis of nanoporous materials such as zeolites and mesoporous molecular sieve, especially the high silica content of fly ash.

### Author Contributions

Ricardo Parra participated in data analysis, designed the study, aided in drafting the manuscript, coordinated the study, methodology, interpreted the results, writing; Carlos Calderón participated in visualization, editing formal, software, data analysis, writing aided in drafting the manuscript, interpreted the results; Jairo Gomez, editing, formal analysis, writing, conceptualization.

### References and Notes

- [1] Szerement, J.; Szatanik-Kloc, A.; Jarosz, R.; Bajda, T.; Mierzwa-Hersztek, M. *J. Clean Prod.* **2021**, *311*, 127461. [\[Crossref\]](#)

- [2] Ren, X.; Xiao, L.; Qu, R.; Liu, S.; Ye, D.; Song, H. *RSC Adv.* **2018**, *8*, 42200. [\[Crossref\]](#)
- [3] Ju, T.; Meng, Y.; Han, S.; Lin, L.; Jiang, J. *Chemosphere* **2021**, *283*, 131010. [\[Crossref\]](#)
- [4] Feng, W.; Wan, Z.; Daniels, J.; Li, Z.; Xiao, G.; Yu, J. *J. Clean Prod.* **2018**, *202*, 390. [\[Crossref\]](#)
- [5] Prado, P.; Nascimento, M.; Yokoyama, L.; Cunha, O. *Am. J. Eng. Res.* **2017**, *12*, 394.
- [6] Yang, L.; Qian, X.; Yuan, P.; Bai, H.; Miki, T.; Men, F. *J. Clean Prod.* **2019**, *212*, 250. [\[Crossref\]](#)
- [7] Amoni, B.; Freitas, ADL.; Bessa, RA.; Oliveira, C.; Bastos, M.; Azevedo, S. *Mater. Chem. Phys.* **2022**, *275*, 125197. [\[Crossref\]](#)
- [8] Lee, Y.; Soe, T.; Zhang, S.; Ahn, J.; Park, MB.; Ahn, W. *Chem. Eng. J.* **2017**, *317*, 821. [\[Crossref\]](#)
- [9] Hu, T.; Gao, W.; Liu, X.; Zhang, Y.; Meng, C. *R. Soc. Open Sci.* **2017**, *4*, 170921. [\[Crossref\]](#)
- [10] Alam, J.; Kumar, V.; Kumar, K.; Cabral, M.; Tavker, N.; Choudhary, N.; Kumar, A.; Abdulraqueeb, F.; Mansour, Alhoshan, M.; Awadh, A. *Crystals* **2021**, *11*, 88. [\[Crossref\]](#)
- [11] Zhang, L.; Yang, F.; Tao, Y. *Fuel.* **2020**, *259*, 116282. [\[Crossref\]](#)
- [12] Kumar, M.; Senthilvadivu, R.; Brahmaji, J.; Neelamegam, M.; Kumar, A.; Kumar, R.; Jena, H. *J. Radioanal. Nucl. Chem.* **2020**, *325*, 971. [\[Crossref\]](#)
- [13] Yousuf, A.; Omer, S.; Youssouf, M.; Malik, Z.; Sajjad, K. *J. Mater. Environ. Sci.* **2020**, *11*, 911. [\[Link\]](#)
- [14] Nowak, P.; Muir, B.; Solinska, A.; Franus, M.; Bajda, T. *Materials* **2021**, *14*, 1558. [\[Crossref\]](#)
- [15] Um, N.; Jeon, T. *Saf. Environ. Prot.* **2021**, *153*, 192. [\[Crossref\]](#)
- [16] Mushtaq, F.; Zahid, M.; Bhatti, I.; Nasir, S.; Hussain, T. *J. Environ. Manage.* **2019**, *240*, 27. [\[Crossref\]](#)
- [17] Bukhari, S.; Behin, J.; Kazemian, H.; Rohani, S. *Fuel.* **2015**, *140*, 250. [\[Crossref\]](#)
- [18] Franus, W.; Wdowin, M.; Franus, M. *Environ. Monit. Assess.* **2014**, *186*, 5721. [\[Crossref\]](#)
- [19] Wang, C.; Yu, J.; Feng, K.; Wang, L.; Huang, J. *Microporous Mesoporous Mater.* **2022**, *345*, 112256. [\[Crossref\]](#)
- [20] Liu, C.; Wang, Y.; Xia, J.; Zhou, L.; Zhang, W.; Zhang, Z. *Energy Sources, Part A.* **2021**. [\[Crossref\]](#)
- [21] Tauanov, Z.; Shah, D.; Inglezakis, V.; Jamwal, PK. *J. Clean Prod.* **2018**, *182*, 616. [\[Crossref\]](#)
- [22] Sivalingam, S.; Sen, S. *Appl. Surf. Sci.* **2018**, *455*, 903. [\[Crossref\]](#)
- [23] Ferrarini, S.; Cardoso, M.; Alban, L.; Pires, M. *J. Braz. Chem. Soc.* **2018**, *29*, 1464. [\[Crossref\]](#)
- [24] Kelechi, S.; Adamu, M.; Uche, O.; Okokpujie, I.; Ibrahim, Y.; Obianyo, I. *Cogent Engineering* **2022**, *9*. [\[Crossref\]](#)
- [25] He, X.; Yao, B.; Xia, Y.; Huang, H.; Gan, Y.; Zhang, W. *Powder Technol.* **2020**, *367*, 40. [\[Crossref\]](#)
- [26] Gjyli, S.; Korpa, A.; Teneqja, V.; Siliqi, D.; Belviso, C. *Environ. Sci. Proc.* **2021**, *6*, 24. [\[Crossref\]](#)
- [27] Adesina A. *Developments in the Built Environment.* **2020**, *4*, 100029. [\[Crossref\]](#)
- [28] Kobayashi, Y.; Ogata, F.; Nakamura, T.; Kawasaki, N. *J. Environ. Chem. Eng.* **2020**, *8*, 103687. [\[Crossref\]](#)
- [29] Xing, Y.; Guo, F.; Xu, M.; Gui, X.; Li, H.; Li, G. *Powder Technol.* **2019**, *353*. [\[Crossref\]](#)
- [30] Harja, M.; Teodosiu, C.; Isopescu, D.; Gencel, O.; Litic, D.; Ciobanu, G.; Cretescu, I. *Materials* **2022**, *15*, 644. [\[Crossref\]](#)
- [31] Alterary, S.; Marei, N. *Journal of King Saud University - Science* **2021**, *33*, 101536. [\[Crossref\]](#)
- [32] Iqbal, A.; Sttar, H.; Haider, R.; Munir, S. *J. Clean. Prod.* **2019**, *219*, 258. [\[Crossref\]](#)
- [33] Yao, Z.; Ji, X.; Sarker, PK.; Tang, J.; Ge, L.; Xia, M. *Earth-Sci. Rev.* **2015**, *141*, 105. [\[Crossref\]](#)
- [34] Tauanov, Z.; Azat, S.; Baibatyrova, A. *Int. J. Coal Prep. Util.* **2020**, *42*. [\[Crossref\]](#)
- [35] Channabasavaraj, W.; Reddy, R. *Int. J. Dev. Res.* **2017**, *7*.
- [36] Blissett, R.; Rowson, N. A. *Fuel* **2012**, *97*, 1. [\[Crossref\]](#)
- [37] Belviso, C. *Ultrason. Sonochem.* **2018**, *43*, 9. [\[Crossref\]](#)
- [38] Onu, C.; O, Nwachukwu. *Global Journal of Researches in Engineering: E Civil And Structural Engineering.* **2022**, *22*. [\[Link\]](#)
- [39] Akin S.; Kirdeciler, S.; Kazanç, F.; Akata, B. *Microporous Mesoporous Mater.* **2021**, *325*, 111338. [\[Crossref\]](#)
- [40] Joseph, I.; Tosheva, L.; Doyle A. *J. Environ. Chem. Eng.* **2020**, *8*, 103895. [\[Crossref\]](#)
- [41] Strzalkowska, E. *Int. J. Coal Geol.* **2021**, *240*, 103746. [\[Crossref\]](#)
- [42] Zhang, Y.; Zhou, L.; Chen, L.; Guo, Y.; Guo, F.; Wu, J.; Dai, B. *Front. Chem. Sci. Eng.* **2020**, *15*, 218. [\[Crossref\]](#)
- [43] Abdelrahman, E.; Alharbi, A.; Subaihi, A.; Hameed, M.; Almutairi, M. A.; Algethami, F. K. *J. Mater. Res. Technol.* **2020**, *9*, 7900. [\[Crossref\]](#)
- [44] Somderam, S.; Abd, Aziz.; Abdullah, A.; Mat, R. *Chem. Eng. Trans.* **2018**, *72*, 325. [\[Crossref\]](#)
- [45] Hamadi, A.; Nabih, K. *J. Chem.* **2018**, *218*, ID 6207910. [\[Crossref\]](#)
- [46] Novembre, D.; Gimeno, D.; Del Vecchio, A. *Sci. Rep.* **2021**, *11*, 13373. [\[Crossref\]](#)
- [47] Rahmawati, C.; Aprilia, S.; Saidi, T.; Budi, T. *Journal of Islamic Science and Technology* **2021**, *7*, 1. [\[Crossref\]](#)
- [48] Jeyageetha, C.; Kumar, S. *Int. J. Sci. Res.* **2016**, *5*, 1688. [\[Link\]](#)
- [49] Irawan, C.; Rumhayati, B. *J. Pure App. Chem. Res.* **2014**, *3*, 88. [\[Crossref\]](#)
- [50] Golewski, G. *Energies.* **2020**, *13*, 2184. [\[Crossref\]](#)
- [51] Nayak, S.; Mohanty, S. *International Journal of Innovative Science and Research Technology* **2019**, *4*.
- [52] Yoldi, M.; Fuentes, E.; Korili, S.; Gil, A. *Microporous Mesoporous Mater.* **2019**, *287*, 183. [\[Crossref\]](#)
- [53] Ke, G.; Shen, H.; Yang, P. *Materials (Basel).* **2019**, *12*, 3895. [\[Crossref\]](#)
- [54] Kunecki, P.; Panek, R.; Wdowin, M.; Bień, T.; Franus W. *Int. J. Coal Sci. Technol.* **2021**, *8*, 291. [\[Crossref\]](#)
- [55] Zhang, Y.; Chen, Y.; Kang, W.; Han, H.; Song, H.; Zhang, C. *J. Clean Prod.* **2020**, *258*, 120736. [\[Crossref\]](#)
- [56] Ni, X.; Sun, X.; Xu, Y.; Xu, D. *J. Mol. Liq.* **2022**, *359*, 119262. [\[Crossref\]](#)
- [57] Langauer, D.; Cabik, V.; Hredzak, S.; Zubik, A.; Matik, M.; Dankova. *Materials* **2021**, *14*, 1267. [\[Crossref\]](#)

## How to cite this article

Parra-Huertas, R.; Calderón-Carvajal, C.; Gómez-Cuaspud, J. *Orbital: Electron. J. Chem.* **2023**, 15, 95.  
DOI: <http://dx.doi.org/10.17807/orbital.v15i2.18260>